Materials for life sciences

Macroporous polyvinyl alcohol-tannic acid hydrogel with high strength and toughness for cartilage replacement

Heng Li[1], Jinming Li[1], Tong Li[1], Chengwei Wu[1], and Wei Zhang[1,*]

[1] *State Key Laboratory of Structure Analysis for Industrial Equipment, Department of Engineering Mechanics, Dalian University of Technology, Dalian 116024, China*

ABSTRACT

Polyvinyl alcohol (PVA) hydrogels as alternative materials for biomedical applications have attracted extensive attention. However, the development of bioactive hydrogel with macroporous structure and good mechanical performance is still an enormous challenge. In this study, a PVA-tannic acid (TA) macroporous hydrogel is presented by cryogelation method. The macropores are obtained by the large-sized ice crystals generated in situ. The pore size of the obtained hydrogel could reach 150–250 μm and the porosity is over 85%. The macroporous PVA-TA hydrogel exhibit notable compressive modulus (0.54 MPa), tensile modulus (0.70 MPa), compressive toughness (1.14 MJ/m^3) and tensile toughness (1.49 MJ/m^3). In addition, the hydrogel has remarkable self-recovery and energy dissipation ability. From the in vitro cell culture, it is observed that TA has strongly enhanced the bioadhesion and bioactivity of hydrogel, implying the potential application of PVA-TA hydrogel in cartilage replacement.

GRAPHICAL ABSTRACT
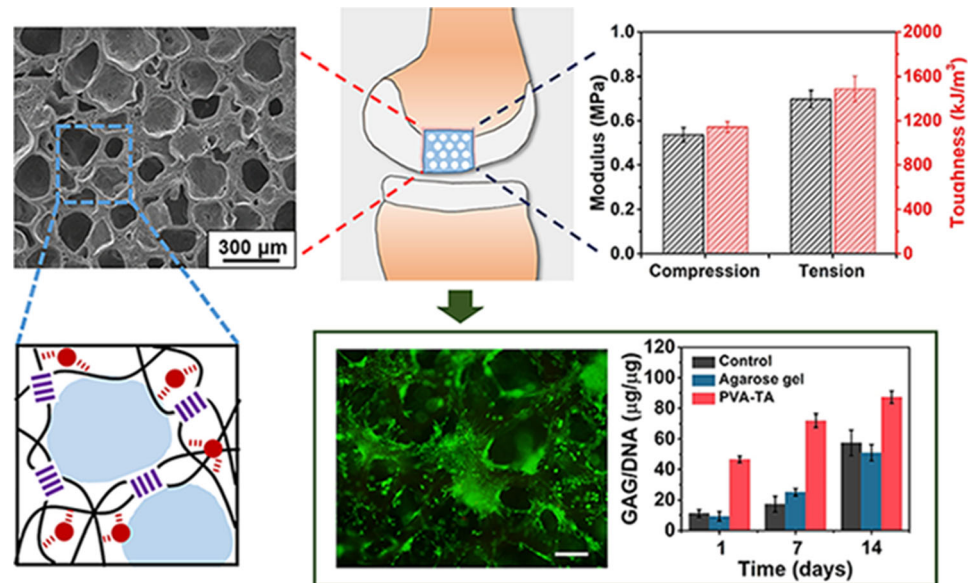
Introduction

Articular cartilage is a highly differentiated connective tissue composed of glycosaminoglycan, collagen matrix and over 75% interstitial fluid [1]. Cartilage plays an important role in dispersing load and reducing friction between joints, showing good compressive, tensile and fatigue resistance. The compressive modulus and tensile modulus are 0.51–1.82 MPa and 0.68–12.49 MPa, respectively [2]. Due to the avascular, aneural and alymphatic nature, cartilage has limited self-repair capacity after injury, requiring the external intervention for cartilage repair [3].

Hydrogel is now the frontline of research in the study of cartilage repair materials. In particular, polyvinyl alcohol (PVA) hydrogels have been extensively studied and drawn much attention in various applications due to their stable chemistry property, water solubility and non-toxicity [4–6]. Especially for physical-crosslinking PVA hydrogel, without introducing toxic reaction solvent in the whole preparation process, it is the promising material in biomedical applications such as wound dressing, tissue regeneration. However, there are still deficiencies restricting PVA hydrogel application. On one side, the physical-crosslinking PVA hydrogel usually has the poor biological activity due to the inherent inert and the micro/nano porous structure, which is inconsistent with the common requirement for cell adhesion and proliferation [7]. On the other side, the physical-crosslinking PVA hydrogel usually does not possess adequate mechanical properties to work in long term load-bearing environment.

The physical-crosslinking PVA hydrogels have been fabricated during freezing–thawing process, where the polymer chains aggregate and crosslink while the solvent forms ice crystals to generate pores. These hydrogels are also called cryogels [8] and the amount and size of ice crystals directly determine the porous morphology. However, it is widely recognized that PVA has a certain inhibition ability to ice crystal formation [9, 10], resulting the pores present in pure PVA cryogels are usually nanoscale [11, 12]. In order to fabricate macroporous PVA cryogel, natural polysaccharides, such as sodium alginate, chitosan and methylcellulose, are blended into PVA hydrogel precursor [13–15]. Though the pore size is increased with respect to pure PVA cryogel, most are still less than 50 μm, which is not sufficient for cell

survival and growth. In our previous work, using agarose (AG) as pore inducing agent, we developed the PVA hydrogel with the pore size 20–200 μm for cartilage repair [16]. But, PVA is not biologically active, which limits the adhesion of hydrogel to chondrocytes and thereby the bio-interaction of the implanted hydrogel with the host cartilage tissue.

Tannic acid, a natural plant-derived polyphenol [17], has been widely introduced to hydrogels to improve the mechanical property and bioadhesion due to the rich of phenolic hydroxyl groups and catechol [18–20]. In this work, TA is introduced to PVA hydrogel to improve the bioadhesion and bioactivity of hydrogels. The chondrocytes cultured in the PVA-TA hydrogel show significant proliferation and continue to secrete extracellular matrix. The obtained PVA-TA hydrogel simultaneously realizes the macroporous structure of 150–250 μm and the comparable mechanical property with natural cartilage, demonstrating its potential application in cartilage repair.

Experimental methods

Material

Poly (vinyl alcohol) (PVA) (polymerization degree: 1750 ± 50, alcoholysis degree: 99.8 –99.9%) was purchased from Sinopharm Chemical Reagent Co., Ltd. China. Tannic acid (TA) ($C_{76}H_{52}O_{46}$, A.R. grade) was supplied by Shanghai Macklin Biochemical Co., Ltd. China. Pluronic® F127 (PF127) was obtained from Sigma–Aldrich, USA. Calcium carbonate ($CaCO_3$) (A.R. grade) and hydrochloric acid (HCl) (A.R. grade) were obtained from Tianjin Kemiou Chemical Reagent Co., Ltd. China.

Preparation of hydrogel

The PVA-TA blend solutions were prepared by dissolving a certain amount of PVA, TA, $CaCO_3$ and PF127 in deionized water (DI water) and stirred at 95 °C for 1.5 h. After the solutions cooled to 40 °C, hydrochloric acid (HCl, 37 wt.%) was added dropwise to produce CO_2 micro bubbles. Gently stirring was performed during the entire process to ensure the sufficient reaction. The amount of each component was shown in Table 1. The hydrogel precursor solution was transferred into a plastic mold, and three times of freezing–thawing procedures were performed (freezing at − 20 °C for 16 h, thawing at room temperature for 8 h). Then, the prepared hydrogels were washed with DI water to remove the possible remnant for the further use.

Scanning electron microscopy (SEM)

The cross-sectional morphology of the hydrogels was evaluated through scanning electron microscopy (SEM, FEI Quanta 200, FEI, USA). All hydrogel samples were frozen in liquid nitrogen to obtain fracture surfaces, and then lyophilized through a freeze drier (FD-1A-50, Yuming, China) over 24 h. Prior to the observation, the surfaces were sputter-coated with a gold layer using a magnetron ion sputter metal coating device (Vacuum Device MSP-1s, Japan). After obtaining the SEM micrographs, the pore size distribution was measured using image analysis software (Nano Measure) by randomly counting the sizes of 100 pores.

Porosity measurement

The porosity of the hydrogel was measured using liquid displacement as reported before [21]. In brief, the hydrogels were immersed in a graduated cylinder containing a known volume V_1 of ethanol, and a series of evacuation-repressurization cycles were conducted to facilitate the penetration of ethanol into hydrogels. Until no bubbles emerged, the total volume of ethanol and the sample immersed in ethanol was recorded as V_2. Then, the sample was removed and the residual ethanol volume was recorded as V_3.

Table 1 Composition and proportion of PVA-TA hydrogel

Sample	PVA (g)	TA (g)	PF127 (g)	CaCO₃ (g)	DI water (mL) (g)	HCl (mL)
PVA	15	–	–	–	85	–
PVA-MB	15	–	1	3	85	3
PVA-1T-MB	15	1	1	3	85	3
PVA-2T-MB	15	2	1	3	85	3
PVA-3T-MB	15	3	1	3	85	3

The porosity ε of hydrogel could be calculated as Eq. 1.

$$\varepsilon = \frac{(V_1 - V_3)}{(V_2 - V_3)} \qquad (1)$$

where $V_1 - V_3$ was regarded as the void volume of the hydrogel, $V_2 - V_3$ was the total volume of the hydrogel.

Swelling property and water content

The swelling ratios were measured using the conventional gravimetric procedure. The hydrogel samples were dried and weighed (m_0). Then, the samples were swollen by immersing in DI water at room temperature and were weighed in the pre-determined time (m_t) after removal of surface water. The swelling ratio (SR) was calculated by Eq. 2.

$$SR = \frac{(m_t - m_0)}{m_0} \times 100\% \qquad (2)$$

The mass of totally swollen hydrogels was denoted as m_s. The water content of hydrogels was calculated through Eq. 3.

$$\text{Water content } (\%) = \frac{(m_s - m_0)}{m_s} \times 100\% \qquad (3)$$

Mechanical property

The uniaxial tension tests were conducted to the barbell shaped hydrogel samples with the strain rate of 300%/min using Sans Universal Testing Machine (Shenzhen SANS Testing Machine Co., Ltd., CMT-4204, China). To increase the friction, the sand paper was sandwiched between the hydrogel and clampers. The tensile stress–strain curves were recorded and the toughness was calculated by the area under curves. The tensile modulus was calculated as the tangent modulus at 10% strain.

The uniaxial unconfined compression tests were performed to hydrogel samples with a strain rate of 30%/min using the same instrument. Prior to testing, the hydrogel samples were totally swollen, and the top and bottom platforms were lubricated with the physiological saline to approximate a pure slip condition. The samples were compressed to 90% strain and the toughness was calculated by the area under the stress–strain curves. The compressive modulus

was calculated from the slope of the 10% to 20% strain.

The compressive loading–unloading cycles were conducted to evaluate the self-recovery ability of PVA-TA hydrogels. The hydrogel samples were compressed to 60% strain for 10 cycles. Besides, the energy dissipation was defined as the area formed by the cyclic loading–unloading curve.

Fourier transform infrared spectroscopy (FT-IR)

Fourier transform infrared spectroscopy was performed using the Attenuated Total Reflection (ATR) mode on a Thermo Nicolet FTIR (Nexus-670) to characterize the functional groups and bonds of the hydrogel samples. The hydrogel samples were vacuum dried and FR-IT spectra were recorded in the wavenumber range of 640–4000 cm^{-1} with the resolution of 4 cm^{-1}.

X-ray diffraction (XRD)

X-ray diffraction studies were conducted on the X-ray diffractometer (XRD-6000, Shimadzu, Japan) using a Cu K_α radiation. The XRD patterns were obtained with a voltage of 40 kV and a current of 40 mA. Samples were loaded into a cavity in a Ni-coated Cu block and diffraction data were collected from 10° to 70° 2θ counting with a scanning rate of 4°/min.

Differential scanning calorimetry (DSC)

Differential scanning calorimetry measurements of hydrogel precursor solutions were performed on a Netzsch differential scanning calorimetry (DSC-204, Germany). 5–10 mg sample was placed in a hermetically sealed aluminum pan. The data was collected from 10 to $-$ 40 °C with a cooling rate of 10 °C/min under nitrogen atmosphere.

The resonance light scattering (RLS)

The resonance light scattering (RLS) spectra were obtained on fluorescent spectrometer (Hitachi, F7000) equipped with a 150 W xenon lamp. The solution under test requires good light transmission, thus the hydrogel precursor is diluted 100 times for RLS testing (PVA solution, TA solution, PVA-TA blend

solutions). Simultaneous scanning was performed in the wavelength of 300–700 nm ($\lambda_{ex} = \lambda_{em}$).

In vitro chondrocyte culture

Rat articular chondrocytes were isolated and cultured in vitro as the previous methods [22]. In brief, cartilage of 4 weeks old rats was harvested from both sides of femoral condyle. The cartilage was sliced into 1 mm^3 pieces and digested by 0.2 wt.% type II collagenase (Solarbio, China) solution at 37 ℃ for 6 h. The digestion solution was filtrated using a cell strainer (70 μm pore size) to remove the impurities. Subsequently, the chondrocytes were centrifuged, resuspended and cultured in Dulbecco's modified Eagle's medium (DMEM, Gibco, USA) with 10% fetal bovine serum (FBS, AusGeneX, Australia) and 1% Penicillin streptomycin (PS, Gibco, USA) in a humidified 37 ℃ incubator (Thermo HERAcell150, USA) at 5% CO_2 supplemented. The second and third passage of chondrocytes were used in the following experiments.

The PVA-3T-MB hydrogels were used to co-incubate with chondrocytes. Prior to the in vitro study, the hydrogel samples were sterilized with ethanol and UV lights, and then were washed with phosphate buffer saline (PBS, Hyclone, USA) for further use. The chondrocytes were trypsinized, centrifuged and resuspended at the density of 2×10^6 cells/mL in the culture medium, and 20 μL cell suspension was seeded onto each hydrogel sample for co-incubation. The culture medium was replaced every two days.

Cell characterization

Cell viability was investigated by Live & Dead Viability Assay Kit (KeyGEN BioTECH, China). After 1, 7 and 14 days of culture, the co-incubated cells were rinsed with PBS three times and stained with Calcein-AM and Propidium Iodide (PI), and then incubated for 20 min. After washing with PBS again, the samples were observed under a fluorescence microscope (Olympus IX71, Japan).

The morphology of chondrocytes seeded on hydrogels was observed on SEM. The chondrocytes cultured for 14 days were washed, fixed in 2.5% glutaraldehyde, and dehydrated by increasing concentrations of ethanol (30, 50, 75, 90, 100% twice). After freeze drying, the morphology was examined on SEM (FEI Quanta 200, FEI, USA).

Biochemical analysis

To determine the capacity of cartilage ECM secretion on PVA-TA hydrogel, the content of DNA and glycosaminoglycan (GAG) were quantitatively analyzed. After the predetermined time, the cell-hydrogel constructs were digested with papain solution at 60 ℃ overnight (0.25 mg/mL in 0.2 mol/L sodium bicarbonate, 0.01 mol/L EDTA, and 5 mmol/L L-cysteine, Solarbio, China). The DNA content was measured using the DNA Quantitation Kit (Sigma-Aldrich, USA). In brief, the DNA content was evaluated using Hoechst 33,258 and the fluorescence was measured at 360 nm excitation and 460 nm emission with a microplate reader (SpectraMax M2e, Molecular Devices, USA).

Glycosaminoglycan (GAG) contents were tested using dimethylmethylene blue (DMMB) dye with the Blyscan GAG Assay Kit (Biocolor, UK). To determine the GAG content both in external and internal chondrocytes, the papain digest and cell culture medium were mixed with DMMB solution and the resultant absorbance was read at 656 nm with a microplate reader.

Statistical analysis

The experimental results were expressed as means ± standard deviations. One-way ANOVA analysis of variance was applied to determine the statistical significance of the differences observed between groups. $p < 0.05$ was accepted as statistically significant.

Result

Morphology characterization

The morphology of PVA and PVA-TA hydrogels are given in Fig. 1. For pure PVA hydrogel, there are lots of pores less than 1 μm. After the introduction of TA and micro-bubbles, the morphology of PVA-TA hydrogel changes obviously. It is found that a few round and sparse pores in PVA-MB and PVA-1T-MB (Fig. 1b and c), which can be attributed to fewer bubbles remaining in the hydrogel formation, since bubbles rise, fuse and collapse. As the TA amount is increased, the sparse pores with ∼ 100 μm are observed in PVA-2T-MB (Fig. 1d). The macroporous
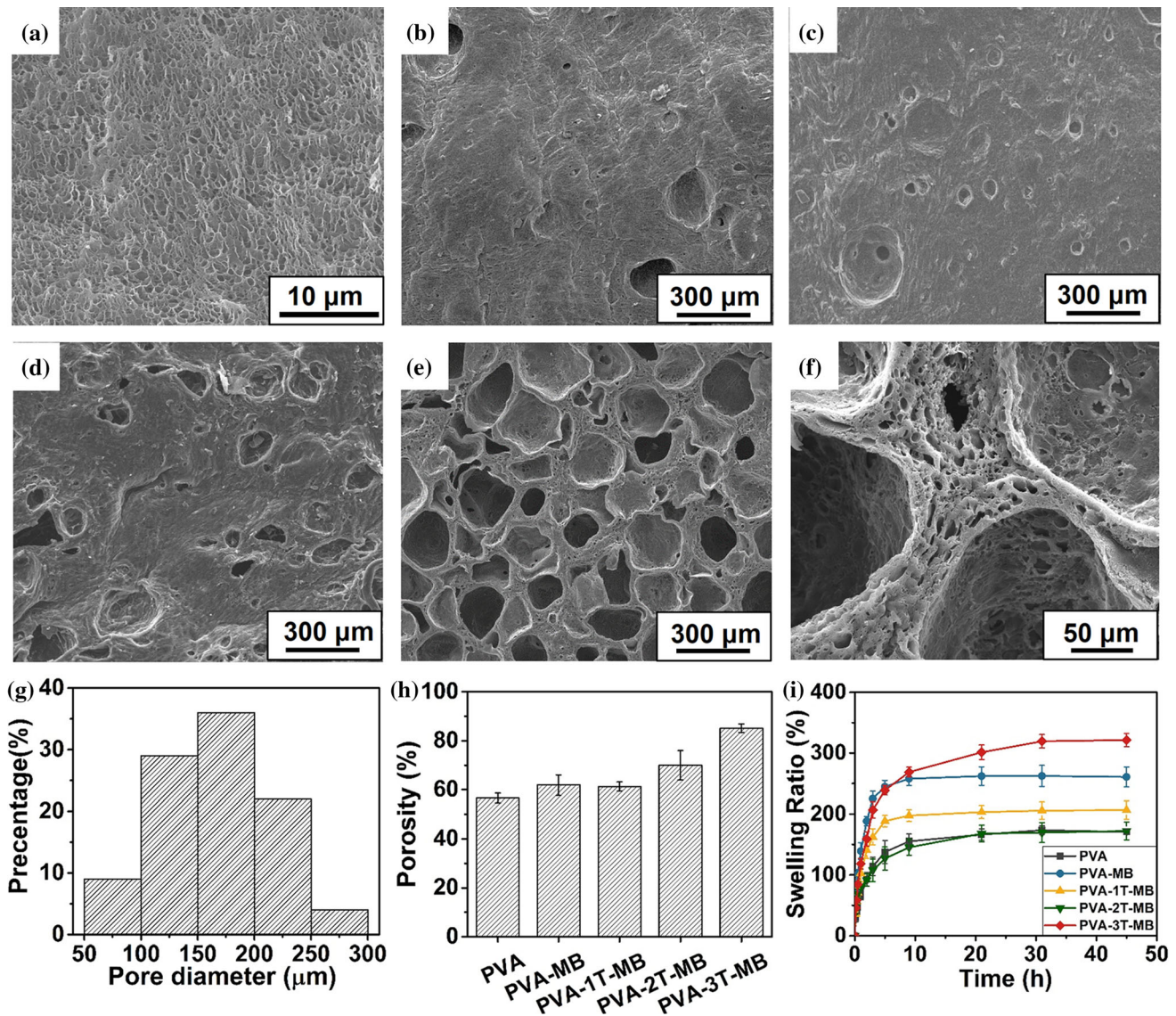
Figure 1 The SEM micrographs of cross-sectional morphology of pure PVA hydrogel (**a**), PVA-MB (**b**), PVA-1T-MB (**c**), PVA-2T-MB (**d**) and PVA-3T-MB (**e**, **f**). The pore size distribution of PVA-3T-MB (**g**). The porosity (**h**) and swelling property (**i**) of hydrogels.

hydrogel with stable pore sizes of 150–250 μm is successfully fabricated with 3 wt.% TA, and the pore distribution is uniform with thinner pore walls, see Fig. 1e, g. In addition, the micropores with several microns are noted on hydrogels ensuring the pore connectivity, shown in Fig. 1f. In addition, the morphology of PVA-3T hydrogel prepared without micro-bubbles shows the spare pores with several hundred microns (Fig. S1), which proves that TA and micro-bubbles must be presented simultaneously to fabricate macropores, and the detailed mechanism will be discussed in discussion section afterwards. The porosity of hydrogel samples is increased

(Fig. 1h) by the introduction of TA, similar with the SEM images. The porosity of PVA-3T-MB reaches 85.07%, 1.5 times higher than that of pure PVA hydrogel.

Furthermore, the swelling properties of PVA-TA hydrogels were tested and the results are shown in Fig. 1i. For all hydrogels, the initial swelling rate is fast and then slows down gradually. The equilibrium swelling ratio is influenced by the pore structure and the density of crosslinking networks in hydrogel. The PVA-3T-MB has the highest equilibrium swelling ratio, which can be ascribed to its interconnected macroporous structure. PVA-MB hydrogel also has a

relatively high swelling ratio due to the weak PVA crosslinking network. For PVA-2T-MB, the equilibrium swelling ratio is the lowest due to its compact PVA-TA crosslinking network and no interconnected pore structure. The equilibrium water content of all the hydrogels can reach ∼ 80% (Fig. S2), which is suitable for biomedical applications.

Mechanical properties

The results of the uniaxial tensile tests of pure PVA hydrogel and PVA-TA hydrogels are shown in Fig. 2a, b. After the incorporation of micro-bubbles, the mechanical properties of PVA-MB decrease sharply. With increasing concentration of TA, though the microstructure change, the tensile modulus,
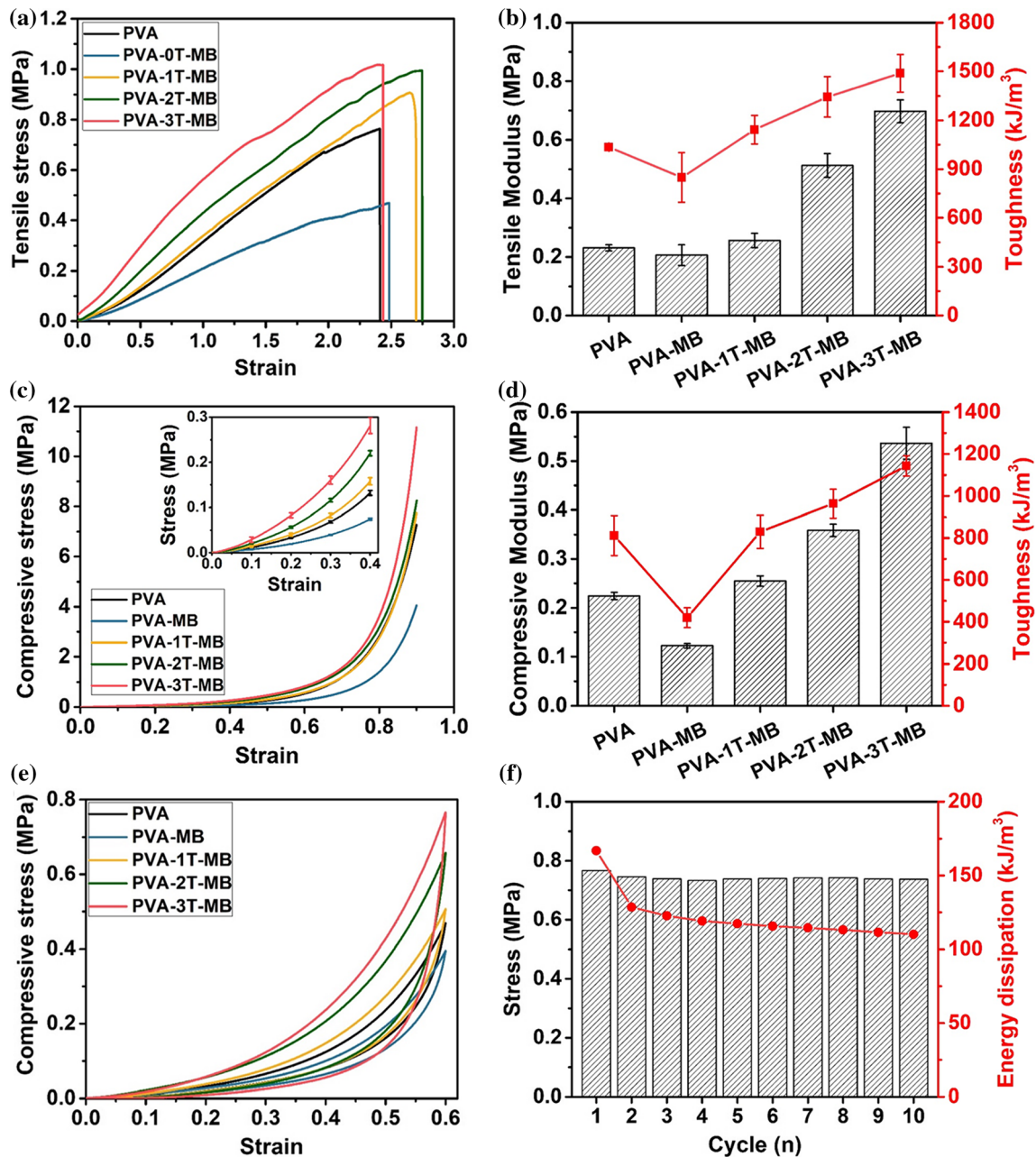

Figure 2 The a tensile stress-strain curves, b tensile modulus and toughness, c compressive stress-strain curves, d compressive modulus and toughness of PVA hydrogel and PVA-TA hydrogels with different TA content. e Cyclic compressive loading-unloading curves at 60% strain. f The maximum stress and energy dissipation of PVA-3T-MB hydrogel through 10 times compressive loading–unloading cycles at 60% strain.

strength and toughness of PVA-TA hydrogels gradually increase. The tensile modulus of the PVA-3T-MB is up to 3 times higher than that of pure PVA hydrogel (0.70 MPa vs. 0.23 MPa). The tensile strength of PVA-3T-MB is enhanced to 1.02 MPa, but the elongation is not improved as the macroporous structure could be regarded as defect in bulk material. Furthermore, the toughness of PVA-3T-MB is 1.49 MJ/m^3, exhibiting notable toughness.

The characterization of the compressive behavior of the hydrogel samples is also carried out and the results are depicted in Fig. 2c, d. Upon compression to 90% strain, all hydrogels do not show significant damage. PVA-3T-MB hydrogel shows a compressive stress up to 11.16 MPa at 90% strain. Moreover, both the compressive modulus and toughness of the hydrogel increase with TA concentration. The PVA-3T-MB hydrogel exhibits compressive toughness as high as 1.14 MJ/m^3 while it maintains a high modulus of 0.54 MPa, which is 2.5 times higher than that of pure PVA hydrogel.

It's an essential requirement for a cartilage repair material to withstand the repetitive loading. To investigate the recovery behavior, the cyclic compressive loading–unloading tests are performed. As shown in Fig. 2e, the compressive loading–unloading curves of these hydrogels show significant hysteresis loops, especially larger of PVA-3T-MB, suggesting that PVA-3T-MB hydrogel dissipates energy much more efficiently. Ten times cyclic compressive loading–unloading tests at 60% strain were further performed and the results are plotted in Fig. S3. The macroporous PVA-3T-MB hydrogel exhibits excellent self-recovery ability. The maximum stress and energy dissipation in the first cycle are 0.77 MPa and 166.87 kJ/m^3, respectively. After 10 successful loading–unloading cycles, the maximum stress and energy dissipation still remain to be 0.74 MPa and 110.05 kJ/m^3, respectively. It seems that the introduction of TA significantly enhances the fatigue resistance of the hydrogel. Furthermore, the macroscopic observation reveals that the shape and height of macroporous PVA-3T-MB hydrogel samples show marginal change after ten cycles of compression loading–unloading (Fig. S4), indicating that there is insignificantly plastic deformation during loading. The results of all the mechanical tests demonstrate that the strength, toughness and fatigue resistance of macroporous PVA-TA hydrogel are significantly enhanced.

FT-IR analysis

FT-IR spectra of PVA, TA and PVA-TA hydrogels with different TA contents were performed and the results are illustrated in Fig. 3a. For TA, The broad absorption band at 3395 cm^{-1} is attributed to the stretching vibration of hydroxyl groups. The characteristic peaks at 1612 and 1533 cm^{-1} for aromatic C = C stretching vibration, the peak at 1717 cm^{-1} for C = O groups and the peak at 1200 cm^{-1} for C-O vibration are observed [23, 24]. As TA blended into hydrogels, these characteristic peaks appear at PVA-1T-MB, PVA-2T-MB and PVA-3T-MB, indicating that TA molecules can be easily blended in the composites. For pure PVA hydrogel, the broad absorption band of –OH stretching vibration is observed at 3246 cm^{-1}. With the incorporation of TA, the –OH bands of PVA-TA shift to lower wavenumber (3241 cm^{-1} of PVA-1T-MB, 3235 cm^{-1} of PVA-2T-MB, 3229 cm^{-1} of PVA-3T-MB). It is well known that the formation of intermolecular hydrogen bonding reduces the force contants of the chemical constants and hence contributes to lower shift of wavenumber [25, 26]. The significant shifts of the –OH bands to lower wavenumbers indicate the formation of strong hydrogen bonding between PVA and TA.

XRD analysis

The XRD tests are performed to evaluate the PVA crystallinity and the patterns of hydrogel samples are shown in Fig. 3b. The XRD pattern of PVA shows three typical peaks at 19.6°, 22.7° and 40.8°, corresponding to the (101), (200) and (102) planes of PVA crystallines [27], while TA shows the amorphous nature as its XRD pattern displays a blunt peak centered at 25°. Due to the existence of Ca^{2+} introduced by CaCO$_3$, the intensities of three typical peaks of PVA-MB weaken, indicating that Ca^{2+} has a weakening effect on the crystallization of PVA [28]. After the introduction of TA, the intensity of peak of (101) plane of PVA crystalline weaken gradually as the TA content increases. The relative intensity of peaks of (101) and (200) planes has changed and the corresponding 2θ degree has left shifted. These results indicate that PVA-TA hydrogels do not show a typical crystalline structure, indicating the strong hydrogen bonding between PVA and TA prevents the crystallization of PVA.

Figure 3 The FTIR spectra (**a**) and XRD pattern (**b**) of hydrogel samples: TA powder (**i**) pure PVA hydrogel (**ii**), PVA-MB (**iii**), PVA-1T-MB (**iv**), PVA-2T-MB (**v**) and PVA-3T-MB (**vi**). (**c**) The RLS spectra of diluted PVA solution, TA solution, PVA-TA blend solutions with different TA contents. (**d**) The DSC thermograms of hydrogel precursors from 10 to − 40 °C.
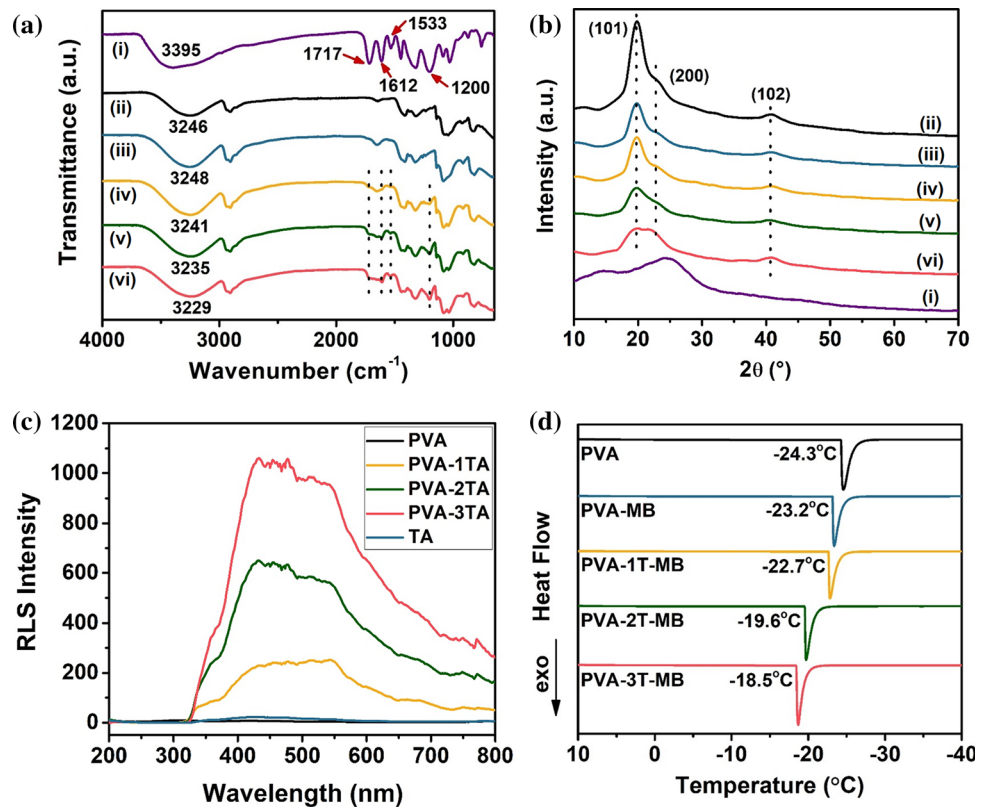
RLS analysis

As reported above, it is identified that there are strong intermolecular hydrogen bonds between TA and PVA. To further investigate the effect of hydrogen bonds on the PVA molecular chain, the resonance light scattering (RLS) is applied to characterize the intermolecular interaction and the molecular chain state. Under illumination, the phenomenon of light scattering is caused by the existence of uneven small 'local aggregation' with irregular distribution in the medium, and the scattering intensity can be used to judge the degree of molecular aggregation in the solution. The experimental result plotted in Fig. 3c shows that almost no light scattering occurs in pure PVA solution or TA solution. When blended with TA, the light scattering phenomenon enhances sharply. In addition, with the increase of TA content, the RLS intensity further increases. This implies that the existence of TA has resulted in the PVA molecular aggregation in the blend solution.

Pore-forming analysis

As shown in Fig. 1d, e the macropores show irregular shape. To explore the pore forming mechanism, the morphology of PVA-3T-MB hydrogel in frozen state is further performed (Fig. S5). It can be seen that the ice particles with the size about 200 μm are closely arranged and embedded in the hydrogel matrix, which is consistent with the microstructures of hydrogel observed via SEM. As such, it is postulated that ice particles work as porogen in pore-forming process of macroporous PVA-TA hydrogel.

To further investigate the effect of TA and micro-bubbles in ice particles formation, DSC experiments are conducted and the thermograms are illustrated in Fig. 3d. The crystallization (freezing) temperature of the hydrogel precursor solutions was estimated from the cooling traces of DSC thermograms. In all curves, one exothermic peak representing heterogeneous ice nucleation is observed. Pure PVA solution exhibits a water crystallization ability at − 24.3 °C. As micro-bubbles are introduced, the crystallization occurs at a higher temperature (PVA-MB: − 23.2 °C). Furthermore, the crystallization temperatures of PVA-TA blend solutions with micro-bubbles increase as a

function of TA content. For PVA-3T-MB, the crystallization temperature reaches $-18.5\ °C$. It seems that both micro-bubbles and TA can enhance the ice formation ability in the blended hydrogel precursor, resulting in the large-sized ice crystals to fabricate macroporous.

In vitro biocompatibility

The biocompatibility of PVA-TA hydrogel as a cartilage scaffold was tested with a live & dead viability assay. As shown in Fig. 4a after 14 days in vitro culture, a large number of living cells stained green

Figure 4 **a** Live/dead analysis for chondrocytes seeded on PVA-3TA hydrogels after 1, 7 and 14 days post seeding. Images display live cells (green) and dead cells (red). The scale bars represent 100 μm. **b** SEM image of chondrocytes cultured on PVA-3T-MB hydrogels. Quantitative analyses of **c** DNA, **d** GAG after 1, 7 and 14 days post seeding compared to the monolayer culture control group and agarose gel group ($n = 3$, $*p < 0.05$; $**p < 0.01$; $***p < 0.001$).
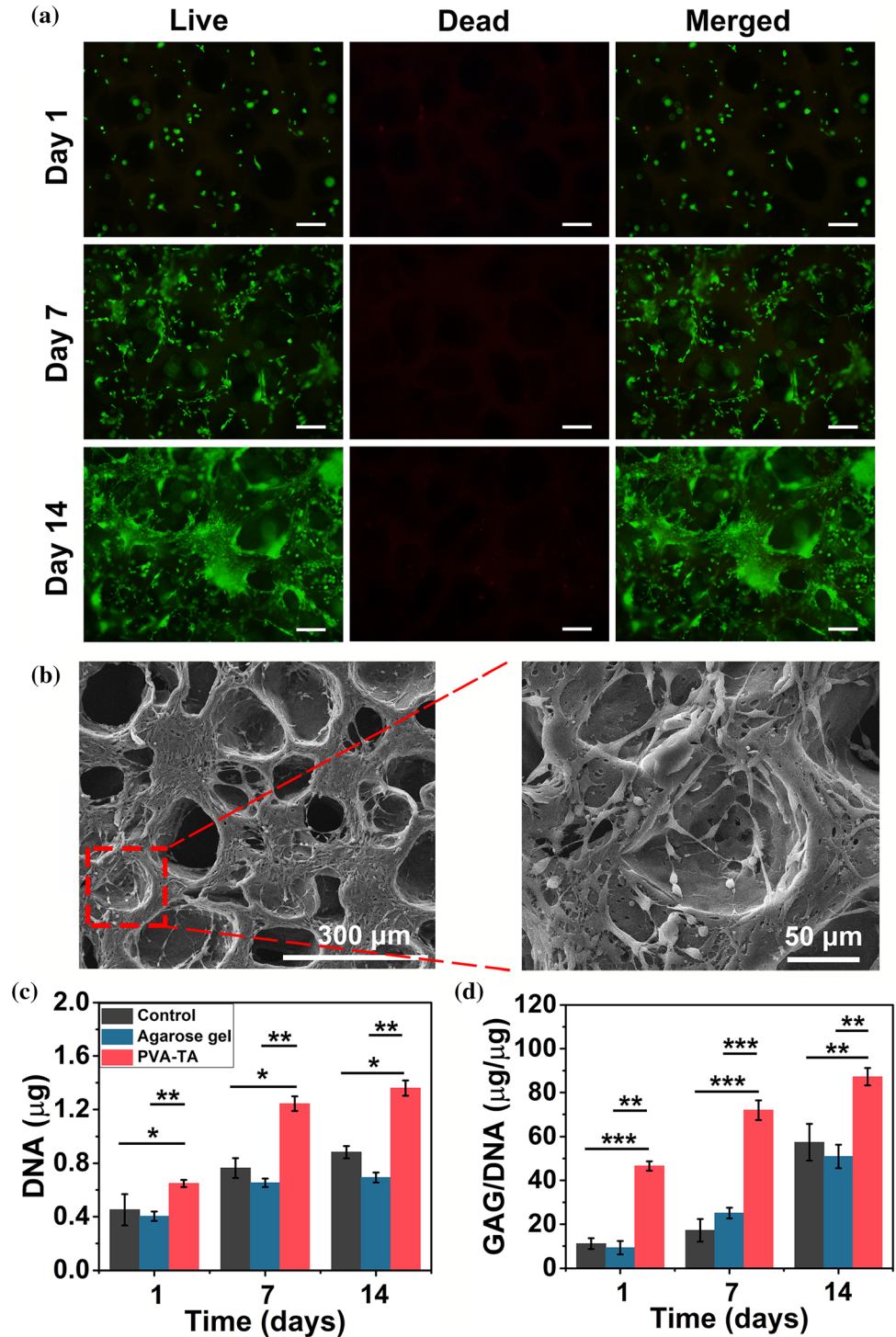
can be observed with nearly no dead red cells visible, and significant cell proliferation occurs with the culture time. The morphology of chondrocytes on the scaffold was observed by SEM, and the results are shown in Fig. 4b. The chondrocytes grow on the surface of the hydrogel and inside the pores, and the significant secretion of extracellular matrix could be observed.

To further evaluate the proliferation and the ability of matrix secretion of chondrocytes in the PVA-TA hydrogel scaffold, quantitative assessments of DNA and cartilage matrix synthesis GAG were carried out. Monolayer culture was used as the 2D culture control group, and agarose gel, a common substrate for cell culture in vitro, was used as the 3D culture control group. The results of DNA contents plotted in Fig. 4c illustrate that chondrocytes exhibit good adhesion and proliferation on the PVA-TA scaffold. After 14 days culture, the DNA content of the PVA-TA hydrogel group is 154.07% and 196.22% of that of the monolayer control group and the agarose gel group, respectively. Furthermore, the ability of GAG synthesis in PVA-TA group is significantly stronger than that of two control groups. When normalized to DNA content, after 14 days culture the GAG synthesized is 87.23 µg/µg for PVA-TA group, which is 1.8 times and 1.2 times higher than 2D culture control group and agarose gel group. It indicates that the chondrocytes cultured in PVA-TA hydrogel have remarkable ability in promoting GAG synthesis. Moreover, it is observed that both the collagen and type II collagen contents of the chondrocytes cultured in macroporous PVA-TA hydrogel increase with the culture time (Fig. S6). It is demonstrated that macroporous PVA-TA hydrogels have the excellent biocompatibility and bioactivity as a result of both 3D macroporous structure and the presence of TA.

Discussion

The experimental results suggest that the prepared PVA-TA hydrogels have the required factors for cartilage repair materials: (i) interconnected porous structure with suitable pore size; (ii) comparable mechanical properties with nature cartilage; (iii) good biocompatibility and bioactivity.

It is demonstrated that the macropores in PVA-TA hydrogels are obtained from the in situ generated large-sized ice particles (around 200 µm) during freezing process. As reported in PVA-AG hydrogel, the large-sized ice crystals formed are mainly due to the large amount of interacting-water aggregated by agarose particles. For PVA-TA hydrogel, the introduction of TA and micro-bubbles play important roles in improving ice particle formation, and this mechanism will be discussed. In hydrogel precursor, due to the abundance of pyrogallol and catechol groups, TA can easily form hydrogen bonding with PVA, altering the state of molecular chains and leading to the local aggregation of PVA molecular chains. During freezing, as the aggregated PVA chains are locally compact, the steric hindrance of ice crystals growth is reduced, enabling the ice crystal to grow further. The stable presence of micro-bubbles in hydrogel precursor is verified (Fig. S7). DSC results have demonstrated that micro-bubbles can improve the formation ability of ice crystals in solution. It can be explained that the micro-bubbles can serve as ice nuclei, and also the interfacial free energy of micro-bubbles can provide energy for ice nucleation[29]. On the basis of the same freezable water, the increase in nucleation sites can ensure the number of ice crystals and control the size of formed ice crystals. The combination of TA and micro-bubbles breaks the inhibition of PVA on ice crystal, and promotes the nucleation and growth of large-sized ice particles, which work as porogen to form the macroporous hydrogels.

For hydrogels, the existence of macropores greatly weakens the mechanical properties of hydrogels. Most macroporous hydrogels have low stiffness and break easily, severely restricting their applications in cartilage and bone regeneration scaffolds [30, 31]. In our study, the compressive and tensile modulus of macroporous PVA-TA hydrogel are 0.54 MPa and 0.70 MPa, and the toughness reach 1.14 MJ/m^3 and 1.49 MJ/m^3, achieving a balance between macroporous structure and considerable mechanical properties. These mechanical properties, especially toughness, are excellent among the hydrogels with similar macropores [32–35]. Sedlačík et al.[36] designed the double network supermacroporous hydrogel, the compressive modulus and strength are up to ∼ 100 kPa and 1 MPa, and tension toughness is up to 38 kJ/m^3. Yue et al.[37] reinforced the polyacrylamide hydrogel with chitin nanofibers and TiO$_2$ nanoparticles. The nanocomposites hydrogel has compressive strength of 1.46 MPa, tensile strength of 316 kPa, and toughness of 47.25 kJ/m^3. Su et al. [38]

obtained the hydrogel with compressive modulus of 0.19–1.38 MPa through the strong intermolecular hydrogen bonding. However, its elongation at break is less than 100% exhibiting the poor tension toughness. Here, the intermolecular hydrogen bonds and polymer chain entanglement caused by PVA and TA have greatly enhanced the mechanical properties of macroporous PVA-TA hydrogel, which is comparable to cartilage [2, 39].

Though PVA is biocompatible, PVA hydrogels usually have poor bioactivity in cell adhesion, proliferation and differentiation due to its biological inertness. The macroporous PVA-TA hydrogel performs good biocompatibility and bioactivity not only due to the porous three-dimensional structure, but also due to the presence of TA. Polyphenols have been extensively explored in many ways for biomedical applications [40] and have been proved to enhance the cell adhesion [41] and promote cell proliferation [42]. As a kind of natural polyphenol, TA improves the bioactivity of the macroporous PVA-TA hydrogel, which is beneficial to its application in cartilage repair.

As discussed above, the introduction of TA can improve the properties of PVA hydrogels to meet the requirements of cartilage repair materials. Firstly, TA can alter the state of PVA molecular chains through the hydrogen bonding to promote the formation of large-sized ice particles during freezing process, which works as the porogen to generate macropores. Secondly, TA can generate strong intermolecular hydrogen bonds with PVA and strengthen the polymer crosslinking network to enhance the mechanical properties of hydrogel. Moreover, the presence of TA strongly improves the bioadhesion and bioactivity of hydrogels, facilitating chondrocytes adhesion, proliferation and matrix secretion.

Conclusion

In this study, the macroporous PVA-TA hydrogel is successfully developed by cryogelation without introducing any toxic substances. The obtained PVA-3T-MB hydrogel has macropores of 150–250 μm with porosity over 85%. Since the addition of TA has dramatically enhanced the hydrogen bonds between PVA and TA, both the strength and toughness are improved to meet the requirement of cartilage, including compressive modulus (0.54 MPa), tensile modulus (0.70 MPa), compressive toughness (1.14 MJ/m³) and tensile toughness (1.49 MJ/m³). More meaningfully, the bioadhesion and bioactivity of the hydrogel are enhanced due to the existence of TA. These results suggest the macroporous PVA-TA hydrogel possesses the promising applications in cartilage repair.

Declarations

Conflict of interest The authors declare that they have no conflict of interest.

Supplementary Information: The online version contains supplementary material available at https://doi.org/10.1007/s10853-022-07209-5.

References

[1] Wei W, Ma Y, Yao X et al (2021) Advanced hydrogels for the repair of cartilage defects and regeneration. Bioact Mater 6:998–1011. https://doi.org/10.1016/j.bioactmat.2020.09.030

[2] Almarza AJ, Athanasiou KA (2004) Design characteristics for the tissue engineering of cartilaginous tissues. Ann Biomed Eng 32:2–17. https://doi.org/10.1023/B:ABME.0000007786.37957.65

[3] Wei W, Dai H (2021) Articular cartilage and osteochondral tissue engineering techniques: recent advances and challenges. Bioactive Materials 6:4830–4855. https://doi.org/10.1016/j.bioactmat.2021.05.011

[4] Baker MI, Walsh SP, Schwartz Z, Boyan BD (2012) A review of polyvinyl alcohol and its uses in cartilage and orthopedic applications. J Biomed Mater Res B Appl Biomater 100B:1451–1457. https://doi.org/10.1002/jbm.b.32694

[5] Sardinha VM, Lima LL, Belangero WD, Zavaglia CA, Bavaresco VP, Gomes JR (2013) Tribological characterization of polyvinyl alcohol hydrogel as substitute of articular cartilage. Wear 301:218–225. https://doi.org/10.1016/j.wear.2012.11.054

[6] Oliveira AS, Seidi O, Ribeiro N, Colaco R, Serro AP (2019) Tribomechanical comparison between PVA hydrogels obtained using different processing conditions and human cartilage. Materials (Basel). https://doi.org/10.3390/ma12203413

[7] Zhang Q, Lu H, Kawazoe N, Chen G (2014) Pore size effect of collagen scaffolds on cartilage regeneration. Acta Biomater 10:2005–2013. https://doi.org/10.1016/j.actbio.2013.12.042

[8] Timothy KL, Henderson MA, Haylock DN, McLean KM, O'Connor AJ (2013) Cryogels for biomedical applications. J Mater Chem B 1:2682–2695. https://doi.org/10.1039/c3tb20280a

[9] Congdon T, Notman R, Gibson MI (2013) Antifreeze (glyco)protein mimetic behavior of poly(vinyl alcohol): detailed structure ice recrystallization inhibition activity study. Biomacromolecules 14:1578–1586. https://doi.org/10.1021/bm400217j

[10] Wang HY, Inada T, Funakoshi K, Lu SS (2009) Inhibition of nucleation and growth of ice by poly(vinyl alcohol) in vitrification solution. Cryobiology 59:83–89. https://doi.org/10.1016/j.cryobiol.2009.04.013

[11] Gutiérrez MC, García-Carvajal ZY, Jobbágy M et al (2007) Poly(vinyl alcohol) scaffolds with tailored morphologies for drug delivery and controlled release. Adv Func Mater 17:3505–3513. https://doi.org/10.1002/adfm.200700093

[12] Jiang S, Liu S, Feng W (2011) PVA hydrogel properties for biomedical application. J Mech Behav Biomed Mater 4:1228–1233. https://doi.org/10.1016/j.jmbbm.2011.04.005

[13] Hou R, Nie L, Du G, Xiong X, Fu J (2015) Natural polysaccharides promote chondrocyte adhesion and proliferation on magnetic nanoparticle/PVA composite hydrogels. Coll Surf B Biointerf 132:146–154. https://doi.org/10.1016/j.colsurfb.2015.05.008

[14] Jiang X, Xiang N, Zhang H, Sun Y, Lin Z, Hou L (2018) Preparation and characterization of poly(vinyl alcohol)/sodium alginate hydrogel with high toughness and electric conductivity. Carbohydr Polym 186:377–383. https://doi.org/10.1016/j.carbpol.2018.01.061

[15] Qi X, Hu X, Wei W et al (2015) Investigation of Salecan/poly(vinyl alcohol) hydrogels prepared by freeze/thaw method. Carbohydr Polym 118:60–69. https://doi.org/10.1016/j.carbpol.2014.11.021

[16] Li H, C-w Wu, Wang S, Zhang W (2020) Mechanically strong poly (vinyl alcohol) hydrogel with macropores and high porosity. Mater Lett 266:127504. https://doi.org/10.1016/j.matlet.2020.127504

[17] Ma S, Lee H, Liang Y, Zhou F (2016) Astringent mouthfeel as a consequence of lubrication failure. Angew Chem Int Ed 55:5887–5891. https://doi.org/10.1002/anie.201601667

[18] Yang S, Zhang Y, Wang T, Sun W, Tong Z (2020) Ultrafast and programmable shape memory hydrogel of gelatin soaked in tannic acid solution. ACS Appl Mater Interf 12:46701–46701. https://doi.org/10.1021/acsami.0c13531

[19] Fan H, Wang J, Jin Z (2018) Tough, swelling-resistant, self-healing, and adhesive dual-cross-linked hydrogels based on polymer-tannic acid multiple hydrogen bonds. Macromolecules 51:1696–1705. https://doi.org/10.1021/acs.macromol.7b02653

[20] Chang M, Liu X, Wang X, Peng F, Ren J (2021) Mussel-inspired adhesive hydrogels based on biomass-derived xylan and tannic acid cross-linked with acrylic acid with antioxidant and antibacterial properties. J Mater Sci 56:14729–14740. https://doi.org/10.1007/s10853-021-06228-y

[21] Zhang R, Ma PX (1999) Poly (α-hydroxyl acids)/hydroxyapatite porous composites for bone-tissue engineering i preparation and morphology. J Biomed Mater Res 44(4):446–455. https://doi.org/10.1002/(SICI)1097-4636(19990315)44:4%3c446::AID-JBM11%3e3.0.CO;2-F

[22] Han G, Shao H, Zhu X et al (2012) The protective effect of xanthan gum on interleukin-1beta induced rabbit chondrocytes. Carbohydr Polym 89:870–875. https://doi.org/10.1016/j.carbpol.2012.04.023

[23] Bai Z, Wang T, Zheng X, Huang Y, Chen Y, Dan W (2020) High strength and bioactivity polyvinyl alcohol/collagen composite hydrogel with tannic acid as cross-linker. Polym Eng Sci 61:278–287. https://doi.org/10.1002/pen.25574

[24] Dai H, Huang Y, Huang H (2018) Enhanced performances of polyvinyl alcohol films by introducing tannic acid and pineapple peel-derived cellulose nanocrystals. Cellulose 25:4623–4637. https://doi.org/10.1007/s10570-018-1873-5

[25] Pretsch E, Buehlmann P, Affolter C, Pretsch E, Bhuhlmann P, Affolter C (2000) Structure determination of organic compounds. Springer. https://doi.org/10.1007/978-3-662-62439-5

[26] Zhang W, Dehghani-Sanij AA, Blackburn RS (2008) IR study on hydrogen bonding in epoxy resin–silica nanocomposites. Prog Nat Sci 18:801–805. https://doi.org/10.1016/j.pnsc.2008.01.024

[27] Peng M, Xiao G, Tang X, Zhou Y (2014) Hydrogen-bonding assembly of rigid-rod poly(p-sulfophenylene terephthalamide) and flexible-chain poly(vinyl alcohol) for transparent, strong, and tough molecular composites. Macromolecules 47:8411–8419. https://doi.org/10.1021/ma501590x

[28] Wang F, Wen Y, Bai T (2016) The composite hydrogels of polyvinyl alcohol-gellan gum-Ca(2+) with improved network structure and mechanical property. Mater Sci Eng C Mater Biol Appl 69:268–275. https://doi.org/10.1016/j.msec.2016.06.084

[29] Heneghan AF, Haymet ADJ (2003) Liquid-to-crystal heterogeneous nucleation: bubble accelerated nucleation of pure supercooled water. Chem Phys Lett 368:177–182. https://doi.org/10.1016/s0009-2614(02)01835-3

[30] Milner PE, Parkes M, Puetzer JL et al (2018) A low friction, biphasic and boundary lubricating hydrogel for cartilage replacement. Acta Biomater 65:102–111. https://doi.org/10.1016/j.actbio.2017.11.002

[31] Zhang S, Li Y, Zhang H et al (2021) Bioinspired conductive hydrogel with ultrahigh toughness and stable antiswelling properties for articular cartilage replacement. ACS Mater Lett 3(6):807–814. https://doi.org/10.1021/acsmaterialslett.1c00203

[32] Chang C, Peng N, He M, Teramoto Y, Nishio Y, Zhang L (2013) Fabrication and properties of chitin/hydroxyapatite hybrid hydrogels as scaffold nano-materials. Carbohydr Polym 91:7–13. https://doi.org/10.1016/j.carbpol.2012.07.070

[33] Fan X, Wang S, Fang Y et al (2020) Tough polyacrylamide-tannic acid-kaolin adhesive hydrogels for quick hemostatic application. Mater Sci Eng C Mater Biol Appl 109:110649. https://doi.org/10.1016/j.msec.2020.110649

[34] Gan D, Wang Z, Xie C et al (2019) Mussel-inspired tough hydrogel with in situ nanohydroxyapatite mineralization for osteochondral defect repair. Adv Healthc Mater 8:e1901103. https://doi.org/10.1002/adhm.201901103

[35] Chang KH, Liao HT, Chen JP (2013) Preparation and characterization of gelatin/hyaluronic acid cryogels for adipose tissue engineering: in vitro and in vivo studies. Acta Biomater 9:9012–9026. https://doi.org/10.1016/j.actbio.2013.06.046

[36] Sedlačík T, Nonoyama T, Guo H et al (2020) Preparation of tough double- and triple-network supermacroporous hydrogels through repeated cryogelation. Chem Mater 32:8576–8586. https://doi.org/10.1021/acs.chemmater.0c02911

[37] Yue Y, Wang X, Wu Q, Han J, Jiang J (2020) Highly recyclable and super-tough hydrogel mediated by dual-functional TiO2 nanoparticles toward efficient photodegradation of organic water pollutants. J Coll Interf Sci 564:99–112. https://doi.org/10.1016/j.jcis.2019.12.069

[38] Su T, Liu Y, He H et al (2016) Strong bioinspired polymer hydrogel with tunable stiffness and toughness for mimicking the extracellular matrix. ACS Macro Lett 5:1217–1221. https://doi.org/10.1021/acsmacrolett.6b00702

[39] Danso EK, Honkanen JT, Saarakkala S, Korhonen RK (2014) Comparison of nonlinear mechanical properties of bovine articular cartilage and meniscus. J Biomech 47:200–206. https://doi.org/10.1016/j.jbiomech.2013.09.015

[40] Zhang X, Li Z, Yang P et al (2021) Polyphenol scaffolds in tissue engineering. Mater Horiz 8:145–167. https://doi.org/10.1039/d0mh01317j

[41] Liskova J, Douglas TE, Beranova J et al (2015) Chitosan hydrogels enriched with polyphenols: antibacterial activity, cell adhesion and growth and mineralization. Carbohydr polym 129:135–142. https://doi.org/10.1016/j.carbpol.2015.04.043

[42] Natarajan V, Krithica N, Madhan B, Sehgal PK (2013) Preparation and properties of tannic acid cross-linked collagen scaffold and its application in wound healing. J Biomed Mater Res B Appl Biomater 101:560–567. https://doi.org/10.1002/jbm.b.32856